Contents

Abstract

1. Belle II e SKB accelerator (SuperKEKB)

In this chapter we will see a summary of the principal physics measurements conducted by Belle II experiment, focusing on the ones which could take particularly advantage from the upgrade of the vertex detector, discussed in this work. We will also go through the structure and the operation of the SuperKEKB accelerator and Belle II detector, to conclude (end) with a short view on the actual state of measurements.

1.1 Physics program of the B-factories

Belle II is a general-purpose experiment, committed to making precision measurements of the Standard Model's parameters (SM) and to searching(looking) for the physics Beyond the Standard Model (BSM). In particular the experiment studies the Charge-Parity (CP) violation in the B mesons system and it also searches for New Physics (NP) evidences in the decays of B and D mesons, in τ leptons and in the dark matter sector (DM), in particular searching for dark photons.

The SM is a physics theory that describe three of the fundamental interactions involving elementary particles, which are(?) strong, weak and electromagnetic [interaction] (excluding/with the exclusion of the gravitational one). It classifies all known particles up to now in 4 main groups: quark, leptons, bosons and Higgs (1.1 on the following page).

Despite its tremendous success achieved over the years, predicting with high precision new particles and mechanisms, unknown until that moment, there are a lot of (many) aspects of the (in) Nature, on which it is unable to give answers. Some of them are listed in the following.

- three generations of quark and leptons are known, but it is not known wheter they should be the only ones and the reasons behind their mass hierarchy.
- Higgs mechanism is able to explain the cause of elementary particles' masses through spontaneous electro-weak symmetry breaking, but it doesn't justify neutrinos' ones (masses).
- SM could also predict other bosons Higgs-like, potentially vector bosons (?), whose existance would be justified in some SUper-SYmmetry theories (SUSY) or others of New Physics.

Figure 1.1: Particle classification in the Standard Model

- Another opened question is the matter-antimatter asymmetry in the Universe. Even though CP violation is necessary to explain the current state of the unievrse, the observed quantity is several orders of magnitude less than needed to explain the matter domination over antimatter, which have allowed the evolution of the universe as we know it today.

- The elements of the Cabibbo-Kobayashi-Maskawa (CKM) matrix, which complex phase is at the foundation of CP violation in the quark flavor sector, are diagonal e it could be suggested the existance of a new symmetry, that exists unbroken at high energy (greater than the order (magnitude) of TeV).

All these opened questions encourage the research of new particles and processes (mechanism) that could give reasonable answers. At the energy frontier, experiments like (such as) Large Hadron Collider (LHC) in Geneve, are looking for new particles created (generated) from the proton-proton collision with a center mass energy up to 14 TeV.
At luminosity frontier instead, the mark (trace) of new particles and mechanisms is searched in precision measurements of suppressed reactions in flavour physics or in the deviations from SM. The discrepancies indeed, could be interpreted as a clue (sign) of new physics beyond SM.
The last is the Belle II approach.

So in the following we will see the main physics channels of Belle II, focusing on those that would benefit the most from the upgrade of the whole detector and in particular of the vertex detector.

1.1.1 Belle II Physics channels

As we will see in chapter 2 (reference), all the proposed upgrades fot the VXD (VerteX Detector) aim to reduce the occupancy levels, increasing the robustness

against trasking efficiency and resolution losses from beam background (section 2.1?). [This implies improved tracking efficiency with $p_T <$ 200 MeV/c.] In particular there are three fundamental aspects in physics performance concern VXD and its upgrade:

- Low momentum track finding;
- Vertex and IP resolution;
- Triggers.

Let's see now (????) the main physics channels in Belle II.

FLAVOR PHISICS

CP-violating phases in quark sector :

- as we mentioned above, the amount of CP violation in the SM is not enough to explain the difference observed between baryon-antibaryon matter. New clues could find studying the difference between B^0 and $\bar{B_0}$ decay rates, so measuring the time-dependent CP violation in penguin transition of b $\rightarrow$ s and b $\rightarrow$ d quarks (such as B $\rightarrow \phi K^0$ and B $\rightarrow \eta' K^0$). In fact in the SM this violation is expected to be very small, so any significant observation of CPV can be interpreted as a signal beyond the SM.
- Also the CP violation in charm mixing, negligible in the SM, could draw attention to new phenomena in the up-type quark sector.
- Another aspect that need to be understood is the large amount of CP violation in the time-integrated rates of charmless hadronic B decays, such as B $\rightarrow K\pi$ and B $\rightarrow K\pi\pi$, observed by other B factories and LHCb.

Ultimate measurements of time-dependent CP violation require a combination of data size and high precision measurement of ΔZ, the distance between the tag and signal in B meson decay vertices. In this respect, the upgrade of the vertex detector could improve a lot the flavor tagging efficiency losses. (??????)

Multiple Higgs bosons : Another fundamental channel is the measurement of the Branching Ratio (BR) of B $\rightarrow \tau\nu$, which is particularly sensitive to the charged Higgs boson (in addition to a neutral SM-like Higgs) that in general couples more strongly to heavier particles, but also of the decay B $\rightarrow D^{(*)}\tau\nu$, where BaBar, Belle and LHCb had already reported some anomalies. Moreover extended Higgs mechanism could introduce extra sources of CP violation. We could notice that semi-tauonic decay measurements, rely on efficient and pure tag side B full reconstruction, and so also on the performance of the Vertex Detector. In general the detection of b $\rightarrow \tau \rightarrow l$ transitions requires good lepton identification below 700 MeV/c (Low momentum track finding).

Flavor Changing Neutral Current (FCNC) :

- For this purpose, measurements of time-dependent CP violation in (...), triple product CP violation asmmetrie in B $\rightarrow$ VV decays, and semileptonic decays B $\rightarrow$ V$l\nu$, V= D^*, ρ are the main approaches.
- It is also important measure b $\rightarrow$ s$\nu\bar{\nu}$ transitions (such as...) which belong to a class of decays with large missing energy.
- ???? Moreover it's necessary to improve FCNC measurements of b $\rightarrow$ d, b $\rightarrow$ s, and c $\rightarrow$ u transitions.

Most analyses with missing energy in the final state utilise hadronic or semileptonic B full reconstruction techniques and the performance of these method is most dependent on low momentum track finding and so on the capabilities of the vertex detector as well.

Sources of Lepton Flavor Violation (LFV) : LFV in charged lepton decay (at rates of 10^{-8}) is a key prediction in many neutrinos mass generation mechanism and other models of physics BSM. Belle II has an unrivalled sensitivity to τ decays, because of their production in a clean (almost) e^+e^- collision background and the large dataset. The experiment analyze τ leptons to search for LF and CP violation and measurement of the electric dipole moment and (g-2) of the τ.

NON FLAVOR PHISICS

Dark Sector : Belle II has a unique sensitivity to dark matter via missing energy decays. Although most research for NP are indirect, there are different model that predict the existance of new particles at the MeV to GeV scale, that couple to the SM via new gauge asymmetries and they also predict a vast range of hidden particles, including dark matter candidates and new gauge bosons.

In these last two areas, τ and dark sectors physics, the aim is to probe forbidden and ultra-rare transition in low-multiplicity final states with as large dataset as possible. This is mostbly rely on trigger efficiency and new trigger strategies, that could take advantage from the upgrade. Many of these processes can only be accesed at Belle II, so it is fundamental increase the perfomance of the detector.

Binding Hadrons : As time goes on, in other B factories and hadron colliders, a large numbers of states not predicted by conventional mesons interpretation, are discovered, changing our understanding of QCD in the low-energy regime. For this reason, study of quarkonia is a fundamental purpose for Belle II. In fact new particles can be produce near resonance, achievable by adjusting the machine energy, or by intial state radiation, which effectively provides a continuum of center of mass energies.

CKM matrix : Belle II is also dealing with the measurements of CKM observable, the matrix elements and their phases, with unprecedented precision.

1.1.2 Vertex reconstruction in Belle II

1.2 SuperKEKB accelerator

The Belle II sensitivity in the precision measurements that we sift throug in the previous section, is feasible expecially thanks to the complexity and the extraordinary performance of the SuperKEKB accelerator which host the (almost) hermetic detector. This complex facility is the result of efforts and efficient collaboration between the researches of KEK laboratory and all the international working groups that partecipate(take part, contribute) to the experiment.

1.2.1 The facility

SuperKEKB is an asymmetric e^+e^- collider with a circumference of 3 km, and a center of mass energy peak equal to $\sqrt{s} = 10.58$ GeV, which corresponds to the mass of the $\Upsilon(4S)$ resonance. Compared to its predecessor KEKB (which started its operation in 1998 and concluded in 2010), the current accelerator has made it possible to obtain the primacy in luminosity ever achieved, equal to $4.7\dot{1}0^{34}cm^{-2}s^{-1}$ in July 2022, using a new scheme to accelerate and collide the beams, through some improvements and additions in the components of the accelerator itself. Moreover the new upgrade of the machine, still under study, will also include (provide for) other intervention expecially to cope with higher background level, in view of further increase of the luminosity.

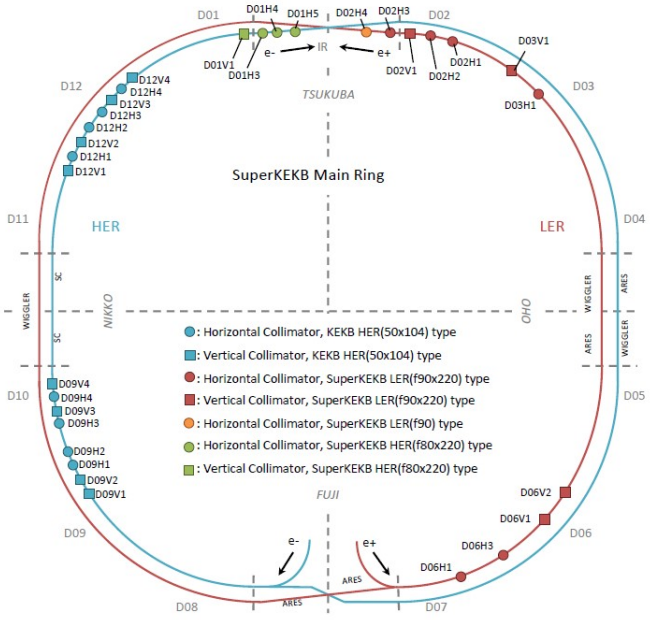

Figure 1.2: SuperKEKB accelerator in 2021. The letters V and H denote respectively vertical and horizontal collimators. Each ring is divided in 12 sections, from the first called D01 to the last D12.

We will briefly see the main features(characteristics) and parameters of the accelerator.

Luminosity

Luminosity is one of the key parameters of an accelerator, it represents the interaction rate per unit of cross section between colliding particles:

$$L = \frac{1}{\sigma}\frac{dN}{dt} \tag{1.1}$$

from which, reversing the equation to obtain N, namely the number of observable physical events:

$$N = \int_0^T L\sigma dt \tag{1.2}$$

where T is the duration of the experiment, σ the cross section of the physical process of interest. (Specifically) In particular luminosity is strictly dependent from machine parameters and from the main features (characteristics) of the beam. With respect to this, it can be expressed as:

$$L = ... \tag{1.3}$$

where .....

As we have already seen, SuperKEKB holds the actual world record in luminosity, with a peak of $4.7\dot{1}0^{34}cm^{-2}s^{-1}$ with β_y^*= 1.0 mm. In the near future the target will be to reach a luminosity of 6.3 $\dot{1}0^{35}$ $cm^{-2}s^{-1}$, increasing current beams and reducing their section in the Interaction Point (IP), squeezing the betatron function up to (a value of??) $\beta_y^* = 0.3mm$. (the monitoring/management) For these reasons, monitoring the beams background becomes one of the most important aspect both to reach the target (goal) and to improve the possible precision measurement of physics.

At the moment (currently, now) it is estimated that the background should remain accettable up to a luminosity value equal to $2{,}8\dot{1}0^{35}cm^{-2}s^{-1}$ with β_y^*= 0.6 mm.

As we shall (?) see, the opportunity (change, possibility) to achieve higher luminosity is closely (strictly) linked (dependent, relate) to an upgrade plan of both the detector and the accelerator.

???????? Most part of the measurements are rare dacays, with small branching fraction, so it is necessary to have a lot of events. [CONTINUA]

Beam energy

Energy beams is mostly decided by the physics program interesting for the experiment. Currently SuperKEKB collides an electron beam with energy of 7 GeV (High Energy Ring, HER) , with a positron beam of 4 GeV (Low Energy Ring, LER), reaching a center of mass energy peaked to Υ(4S) resonance. Also the choice of colliding (using) asymmetric beam (like its predecessor KEKB, which collided (got collide) electrons beam of 8 GeV with a positrons beam of 3.5 GeV) is necessary to identify and measure decay vertices of particles created in the collision. Indeed this mechanism allows to boost the decay products, improving the vertices reconstruction and increasing the sensitivity of the physics measurement, too. In particular this makes possbile time-dependet measurements, expecially in CP violation. We have already seen some of the physics

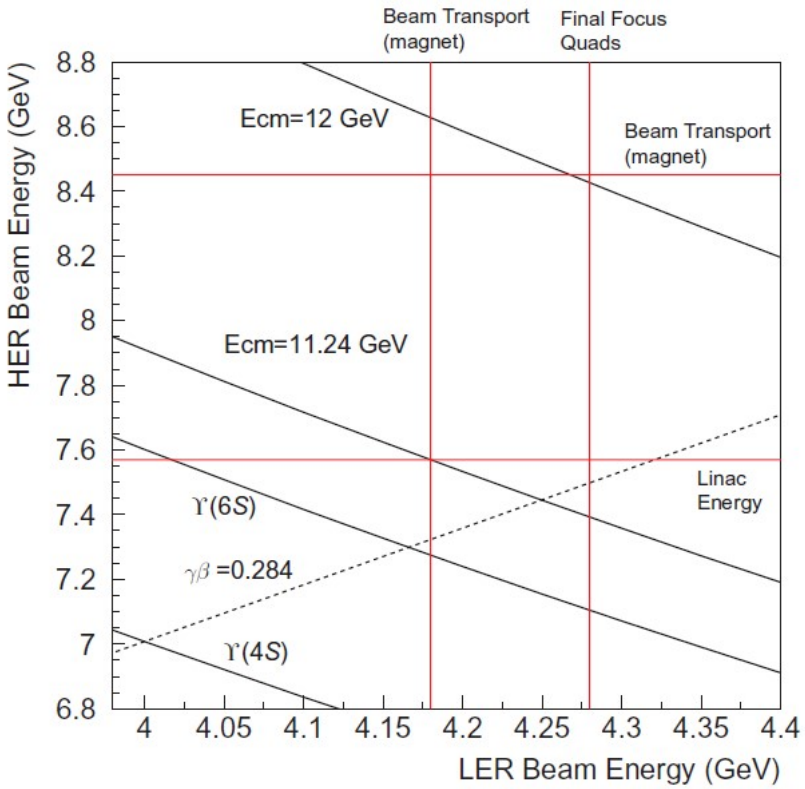

Figure 1.3: Beam energies to reach center of mass energy equal to Υ(4S), Υ(6S),11.24 GeV and 12 GeV. Horizontal axis represents the energy of LER and the vertical one the energy of HER.

behind this choice in section ?????.

In figure **??** on page ?? the flexibility of the energy of both beams LER and HER is showed. The possible range covers energies which goes from the Υ(1S) resonance to the Υ(6S), qith a peak in 11.24 GeV.

1.2.2 "Nano-beam" scheme

[?]

As mentioned in the previous section, a key elemnt to define the luminosity is the *beta function* β in the Interaction Point (IP). To be able to increase luminosity, it's necessary to decrease the value of β depending on the variation of the other machine parameters, but not only, which are part of its definition (richiama equazione con parametri macchina). The mechanism used in SuperKEKB is called *nano-beam scheme*, and it allowed to obtain luminosity 40 times greater than that of KEKB, managing to (succeding) decrease of 1/20 the β function in the IP.

This new scheme, designed by P. Raimondi, dictates that the beams collide at large angle, in SuperKEKB equal to 83 mrad (keeping beams divided through quadruople magnets), in order to reduce the *hourglass effect*, which

succeed when the bunches in the beam are much longer.
We can see briefly the most important parameters that influnce the mechanism?????

The overlap area of the beams is localized and its lenght is given by:

$$d = \frac{\sigma_x^*}{sin\phi_x} \tag{1.4}$$

with ϕ_x defined as half of the crossing angle. The overlap lenght d represent the real lenght of the bunch to consider in the evaluation of the hourglass effect, and it is smaller than the effective bunch lenght along the direction of the beam axis. To reduce this effect, it's necessary to get:

$$\beta_y^* \geq d = \frac{\sigma_x^*}{sin\phi_x} \tag{1.5}$$

Therefore to increase the β function in the IP, the value of d has to diminish, decreasing as aconsequence the horizontal section in the IP and also icreasing the crossing angle. Using a crossing angle large enough, has other positive implications on the operation of the accelerator:

- allows the placement of a new focusing system in the IP with a superconducting quadrupole magnet;
- allows to have two distinct line which host HER and LER beams;
- diminisches the *fringe fields* effect in the IP, wihch are the residuals of the magnets (magnetic fields) in the proximity (nearby).

In figure 1.4 on the facing page are reported the main machine parameters (default value) of the SUperKEKB accelerator.

1.2.3 Background monitoring system

[?]

Background is one of the most important problem for a particle detector, both for precision measurements of physics and for the performance of the different layer detector which constitute (make up) Belle II. For this reason several detectors are used to obtain measurements of radiation dose on both detector and delicate regions of the accelerator, to intervene as soon as possible in case of too high levels are reached. Indeed large doses of radiation could cause accidental damages on the detector, decreasing its performance.

In the chapter 2 (reference) we will go through the main (primary, leading) reasons of background. For now we mention some of the monitoring devices for the backgorund in SuperKEKB.

- Diamonds detector (called "Diamonds') which control the rate of the radiation dose in the interaction region of the beam pipe. These also are part (take part) of the "fast beam abort system", which is a control system that collect (consider) data from different detector to evalute (valutare nel senso di decidere) the beam "turning off", in order to avoid that events out of control could cause damage (harm) to the whole structure.

	LER	HER	Unit
E	4.000	7.007	GeV
I	3.6	2.6	A
N_b	2500		
C	3016.315		m
ε_x	3.2	4.6	nm
ε_y	8.64	11.5	pm
β_x^*	32	25	mm
β_y^*	270	300	μm
$2\phi_x$	83		mrad
α_p	3.25×10^{-4}	4.55×10^{-4}	
σ_δ	8.08×10^{-4}	6.37×10^{-4}	
V_c	9.4	15.0	MV
σ_z	6	5	mm
ν_s	−0.0247	−0.0280	
ν_x	44.53	45.53	
ν_y	44.57	43.57	
U_0	1.87	2.43	MeV
τ_x/τ_s	43.1/21.6	58.0/29.0	msec
ξ_x	0.0028	0.0012	
ξ_y	0.0881	0.0807	
L	8×10^{35}		$\mathrm{cm}^{-2}\,\mathrm{s}^{-1}$

Figure 1.4: Machine parameters of SuperKEKB. The mark "*" indicate values in the IP.

- CLAWS (sCintillation Light And Waveform Sensors), made by scintillator of plastic material and silicon photomultipliers, and used to monitor the Belle II background in the nearby (proximity) of the beam injection (main ring). Together with diamonds it takes part to the beam-abort system.
- TPC's (Time Projection Chambers) which provides measurements (better) on the direction of the neutron flux in the tunnel which hosts (that houses) the accelerator.
- He^3 tubes for the counting of thermal neutrons (which are those with a kinetic energy lower than 1/10 of eV, generally about 0.025 eV) around the Belle II detector.

1.3 Belle II detector

Belle II detector is a general-purpose spectrometers, optimized in precision measurements of B mesons and their decay products. Despite (Compared to) its predecessor Belle, it have to (must) preserve (keep, mantain) good performance despite having smaller boost in the center of mass and undergoing (???) greater levels of background and so of radiations, which are the principal(main) cause of premature degradation of performance and average (mean) life of the detector itself.

Belle II consists of a series of nested subdetectors, which surrounds the IP of the two beams, placed around the berillium beam pipe of 1 cm of radius. Now we will go trough a briefIt description of the several subdetectors.

1.3.1 Vertex Detector (VXD)

1.3.2 Central Drift Chamber (CDC)

1.3.3 Particle identification system (TOP e ARICH)

1.3.4 Electromagnetic calorimeter (ECL)

1.3.5 K_L muon detector (KLM)

1.3.6 Trigger system

1.4 Current state and perspectives of data taking

1.4.1 Alcune ulteriori modifiche rispetto a KEKB

2. Upgrade di Belle II

2.1 Sorgenti di background e limitazioni di Belle II

2.1.1 Effetto Touschek

2.1.2 Beam-gas scattering

2.1.3 Radiative Bhabha scattering e processi a due fotoni

2.1.4 Radiazione di sincrotrone (SR)

2.1.5 Instabilità "Head-tail"

2.1.6 Stato attuale del background e implicazioni future

2.2 Motivazioni per l'upgrade

2.3 Sommario di possibili upgrade

2.3.1 DEPFET

2.3.2 Thin sensor

2.3.3 CMOS MAPS

2.3.4 SOI

3. Il rivelatore VTX

3.1 Layout del rivelatore VTX

3.1.1 iVTX

3.1.2 oVTX

3.2 Simulazioni di performance

3.3 Caratteristiche chip sensore

3.4 Struttura meccanica

4. Sensori CMOS MAPS

4.1 Rivelatori a semiconduttore

4.2 Sensori a pixel monolitici/ibridi

4.3 Tecnologia CMOS MAPS

4.4 Storia degli sviluppi di Monopix

5. TJ-Monopix 2 characterization ??

5.1 Matrix and flavors

5.1.1 Mask (operation) and noisy pixels

5.1.2 Analog and digital readout

5.1.2.1 BCID reset

5.1.2.2 Main registers (and conversion?)

5.1.3 Comparison of trends from data with simulation

To understand how the threshold's value changes with the settings of the chip, we take different measurements varying the values of the main registers which are responsible for it. The results are compared with simultion done by Hung Pham (...).

5.1.3.1 I_{CASN}

This current is responsible of the output baseline. In a few words, higher this value, higher the baseline, lower the threshold and also a little bit the gain.

In figure 5.1 on the next page, we can see the behaviour of the threshold and the gain, increasing the value o I_{CASN}.

To verify this behaviour, we run three different analysis (measurements) by fixing I_{THR} = 20, 40, 64 and changing I_{CASN} from 0 to 30 DAC, with a step of 5 DAC. We have done this enabling 200 pixels in the Cascode FE (rows: 472 - 512, cols: 225 - 230).

For each measurements we fit the threshold distribution with a gaussian function in order to obtain average values of the threshold and its dispersion.

$I_{THR} = 64$:

I_{CASN} [DAC]	THR [DAC]	THR Dispersion [DAC]
0	61.43	2.45
5	53.42	2.45
10	50.33	2.45
15	48.21	2.41
20	46.70	2.38
25	45.49	2.52
30	46.09	2.50

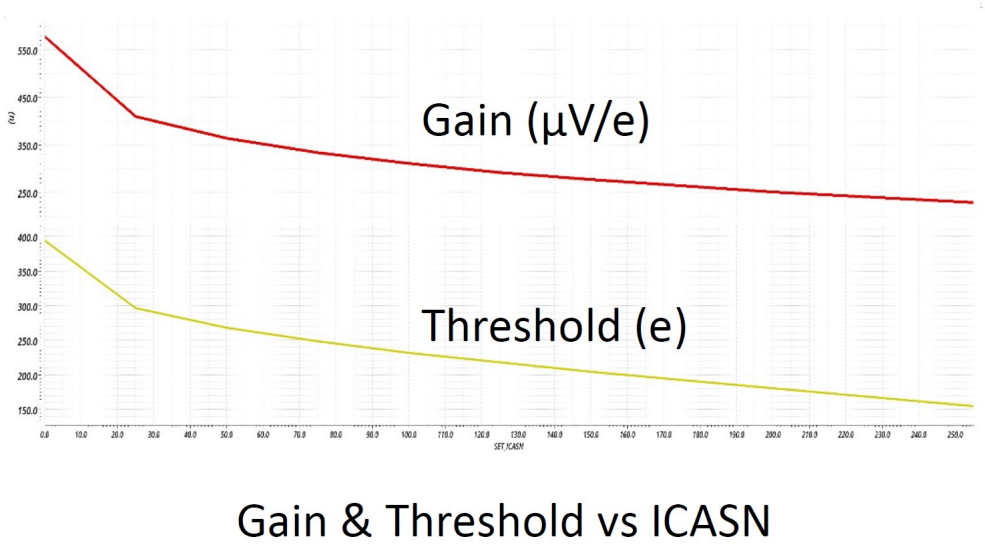

Figure 5.1: Trends of Gain and Threshold increasing I_{CASN}.

$I_{THR} = 40$:

I_{CASN} [DAC]	THR [DAC]	THR Dispersion [DAC]
0	47.28	2.12
5	41.07	2.02
10	38.39	2.03
15	36.65	1.95
20	35.53	1.91
25	NaN	NaN
30	33.37	2.04

Here we can see a particular setting, that is $I_{THR} = 40$ AND I_{CASN}=25, for which the chip doesn't seem to work.

PIXEL THAT FIRE UP??

$I_{THR} = 20$:

I_{CASN} [DAC]	THR [DAC]	THR Dispersion [DAC]
0	34.43	1.95
5	28.10	1.72
10	26.59	1.75
15	24.66	1.77

In figure 5.2 on the following page all trends obtained from these data are reported.

TREND OF DISPERSION?

5.1.3.2 I_{THR}

Reusing the same data of the previous measurements, we can also study the trend of the threshold changing the value of I_{THR} and fixing that of I_{CASN}.

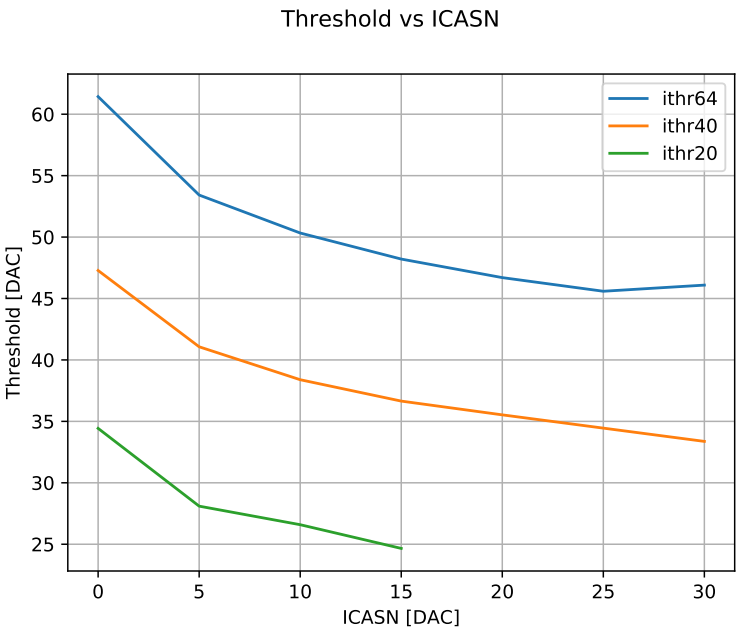

Figure 5.2: Threshold vs. I_{CASN} for I_{THR}= 20, 40, 64.

We consider only I_{CASN} from 0 to 15 DAC, because for highr values we don't have enough values of the threshold (only two, for I_{THR}=40, 64). The results are showed in figure 5.3 on the next page.

We can compare them with the simulation done by Hung Pham (5.4 on the facing page).

5.1.3.3 v_{CASP}???

5.1.3.4 Time over Threshold (ToT)

The last analysis that we have done to make a comparison with the simulations, is about the trend of the ToT, changing the value of I_{CASN} for a fixed value of I_{THR} and vice versa. In particular we consider the data obtained with I_{CASN} fixed to 0 DAC and I_{THR} to 64 DAC, which are the values for this registers, studied and used during the Test Beam in Desy.

5.2 Characterization by injection

In the prototype under test (study), W14R12 chip, some problems (raised up) arose right from the beginning, linked (concerned) pixels of the matrix both for the analog and digital part. Despite its predecessor Tj-Monopix 1, Tj-Monopix 2 is equipped with a circuit which allows the *threshold tuning*.In other words it can adjust, even if only few DAC, every pixel threshold, in order to have a global threshold on the matrix as uniform as possible, or in any case a dispersion as small as possible.

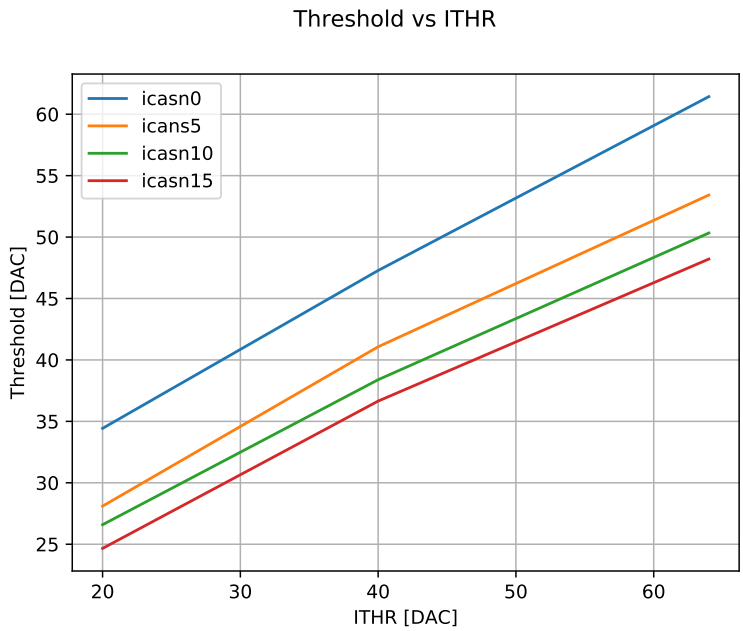

Figure 5.3: Threshold vs. I_{THR} for I_{CASN}= 0, 5, 10, 15.

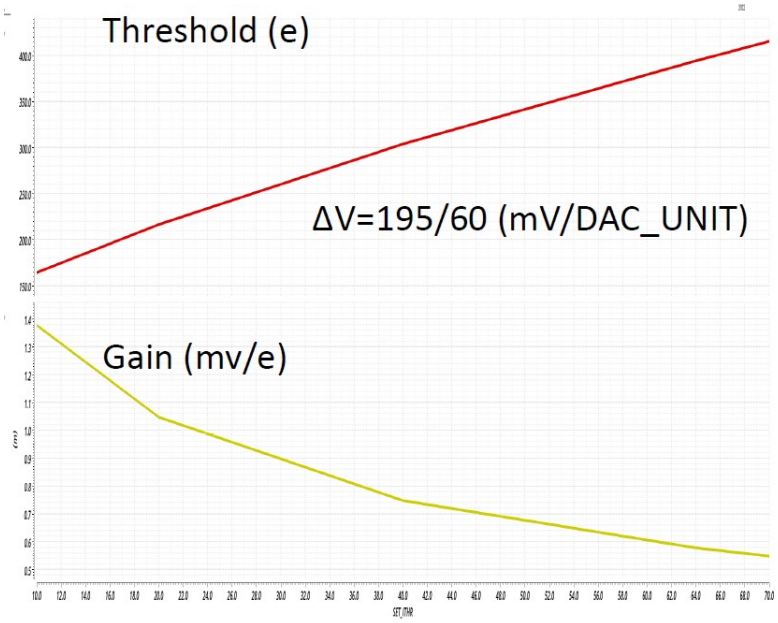

Figure 5.4: Trends of Gain and Threshold increasing I_{CASN}.

Preliminarly it's necessary to study the threshold distribution on the whole matrix. We have separately analyzed the four flavors, to be able to study their main difference in working (performance) and features.

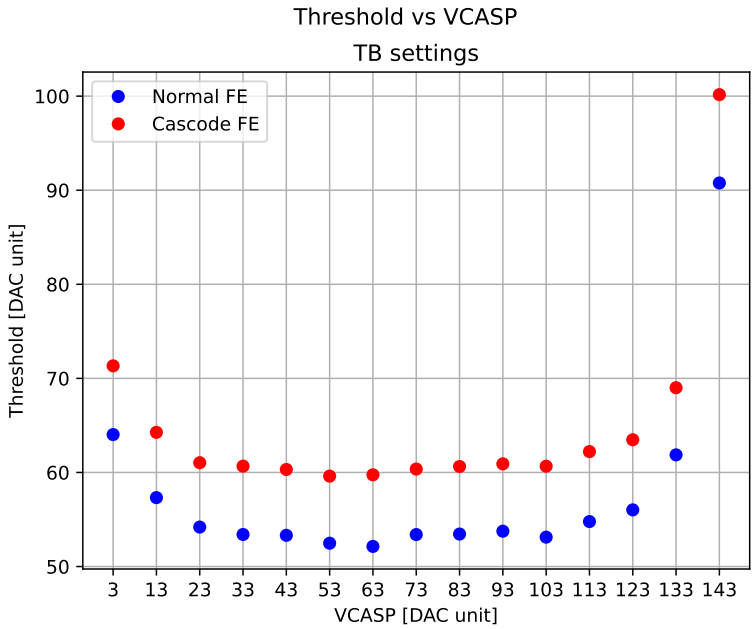

Figure 5.5: Trends of Threshold increasing V_{CASP}.

The ultimate purpose of this measurement is to describe (depict, mark out) the behaviour of each pixel, injecting a charge equivalent to the typical energy released from electrons emitted in radioactive decays (decays of radioactive materials) and in particular those produced by the electronic capture of ^{55}Fe (presente in laboratorio). As explained in the previous section (reference), the ^{55}Fe has an emission spectrum (lines) with lines quite peaked (sharp) and this allows to compare data more easily. The first line is at 5.9 KeV which corresponds on average to about 1616 e^- released (through the pixel??). For this reason during the injection measurement, it's mandatory to know the conversion between DAC and e^- (reference) and to inject charges in order to study pixel behaviour the right region, which are more interesting from a physical point of view.

5.2.1 Injection circuit issues

In carrying out the measurements mentioned above, we noticed (NO) some issues with the injection circuit which limits its working range: (as a matter of fact) the height of the injection pulse is expected to grow (increase) linearly up to a value of (about) $\approx$ 140 DAC, but above this (quantity) value, the circuit increases not only a little the height of the signal, but also the threshold artificially grows by a certain amount of ΔV (or equivalently of ΔQ, related by the conversion factor....REFERENCE). Moreover, for injection height grater than 200 DAC, only the threshold grows, without increasing the actual injected charge in any way.

For this reason, the investigation on the (values) behaviour of the threshold and its dispersion of all flavours of the matrix, required a series of additional measurements.

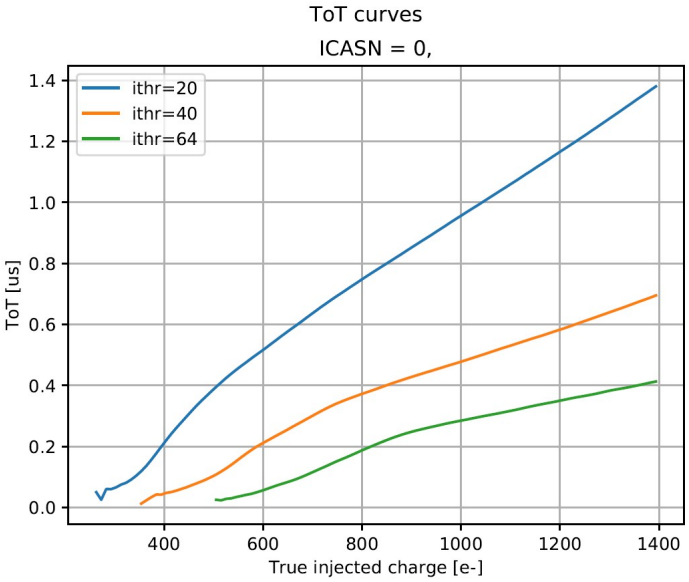

]

(a) ToT vs I_{THR} (I_{CASN}=0 DAC) - Data [**Cascode**

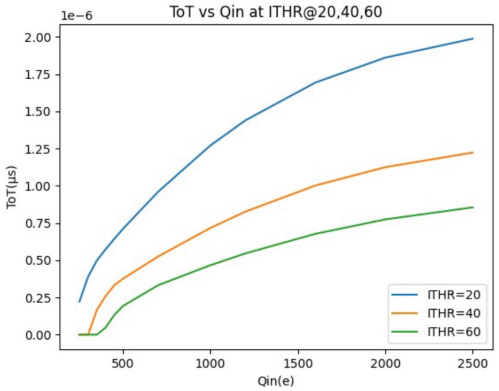

(b) ToT vs I_{THR} (I_{CASN}=0 DAC) - Simulation

Figure 5.6: .

5.2.2 Measurement of the average shift of the threshold value for injected charge greater than 140 DAC

To evaluate this artificial shift of the threshold, two different measurements of the threshold and its dispersion have been done, for each flavor:

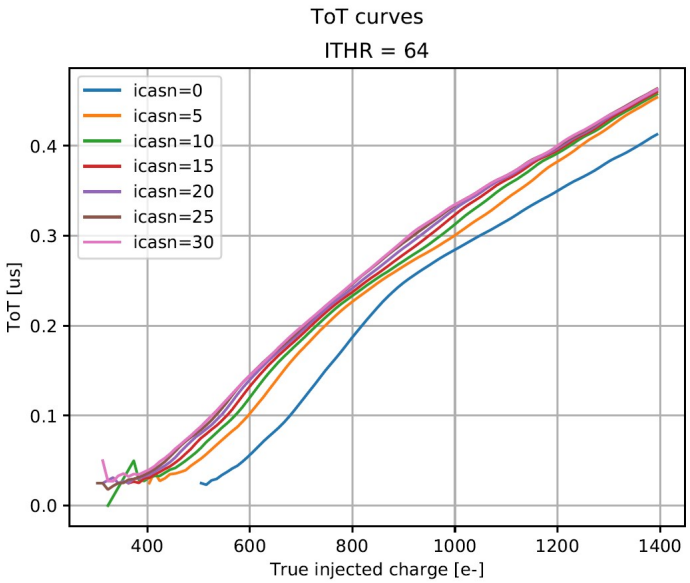

]

(a) ToT vs I_{CASN} (I_{THR}=64 DAC)

-

Data

[**Cascode**

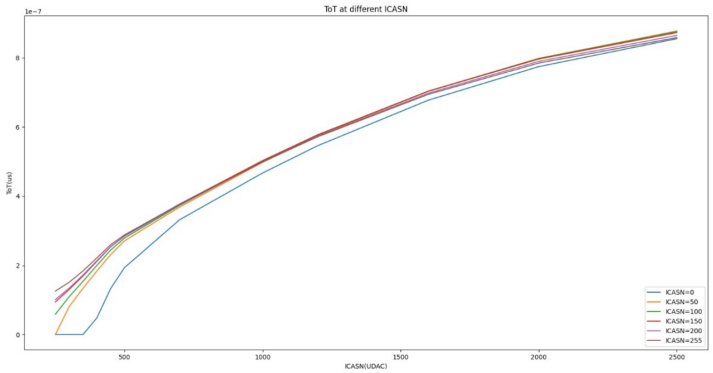

(b) ToT vs I_{CASN} (I_{THR}=64 DAC) - Simulation

Figure 5.7: .

- for an injected charge equal to 140 DAC → before the saturation region;
- for an injected charge equal to 200 DAC → almost the maximum limit of the saturation region (from this value onward only the threshold increases, not the injected charge).

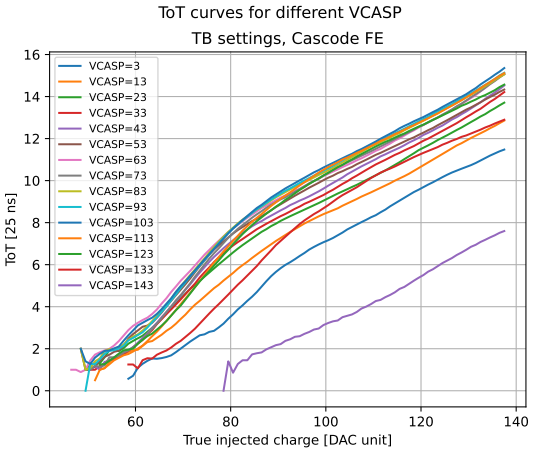

]

(a) ToT vs V_{CASP} - Data [**Cascode**

]

(b) ToT vs V_{CASP} - Data [**Normal**

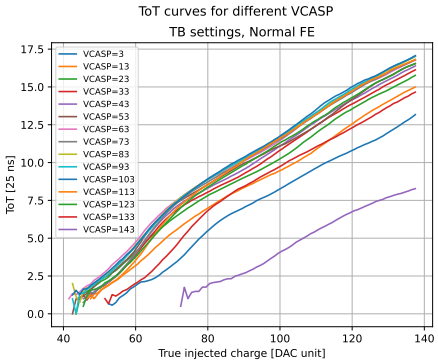

Figure 5.8: .

The threshold distributions obtained from each measurements have been fitted to extract an average value on the whole flavor. Naming $Q_{th,140}$ and $Q_{th,200}$ the threshold obtained from injections of 140 and 200 DAC respectively, the mean shift has been estimated by:

$$\Delta Q = Q_{th,200} - Q_{th,140} \tag{5.1}$$

Eventually, this charge shift has been subtracted from data collected for injection pulses of 200 DAC, in order to extrapolate (deduce) the behaviour of the injected pixels up to a value fo 170 DAC.

What has been obtained for each flavor is reported in the following section, together with a briefly explanation of the method used to estimate (evaluate) the threshold.

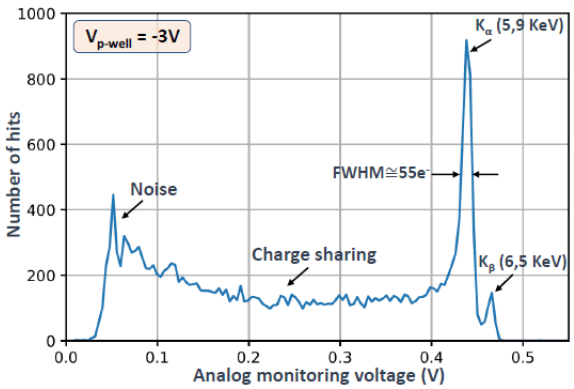

Figure 5.9: ^{55}Fe (radiactive source) emission spectrum using the analog output of a PMOS reset front-end of TJ-Monopix 1. (referenceeeeee)

5.2.3 Threshold and S-Curve

In order to obtain the thresold value for every pixel, each one has to be injected a random (arbitrary) number of times (we have chosen 100 times) for each value of the injection pulse between a minimum value, chosen set the chip register "**VL**" and a maximum value, set by the "**VH**" register, with a random step which is 1 for us.(ANCHE NO)

So with(fixed) the value of the injection pulse fixed, the mean of 100 output are considered. In this way, the typical curve, better known as "*S-curve*", is obtained for each pixel. It is an *error-function* from which the value of the threshold is evaluated considering (taing, extractin, pulling out) the value of the injected charge at half of the curve's maximum height.

Plotting the number of hits observed on each pixel divided by the total number of injections, for each injected charge, the half height corresponds to a charge value for which the pixel detects 50 hits of 100 injected and so when it has an occupancy of 0.5.

In the following are reported the results of this study for the flavors of all matrix.

5.2.3.1 Normal FE

As epxplained in the section (reference) the first flavor of the matrix is the **Normal FE**, which consist of 512 rows (0-511 in registers?) and 224 columns for a total of 114.688 pixels. In figure 5.10 on the next page are plotted all the s-curves of the Normal flavor pixels. The chip registers have been set with the same values used during the Test Beam at Desy (during...) which are reported in table 5.1 on the facing page.

COLORAAAAA

Using this setting, none of the pixels were noisy and so it wasn't necessary introduce (use, ...) any mask.

As already explained in the previous section (reference?) the threshold distributions from the two different measurements with an injection pulse of 140 and 200 DAC respectively, have been fitted and they are showed in figure 30

Registri	Default Settings ("GOE")
ITHR	64
IBIAS	50
VRESET	143
ICASN	0
VCASP	93
VCASC	228
IDB	100
ITUNE	53
VCLIP	255
ICOMP	80
IDEL	88
IRAM	50

Table 5.1: Settings of the main registers used for the W14R12 chip, for Normale and Cascode flavors, during the Test Beam in Desy.

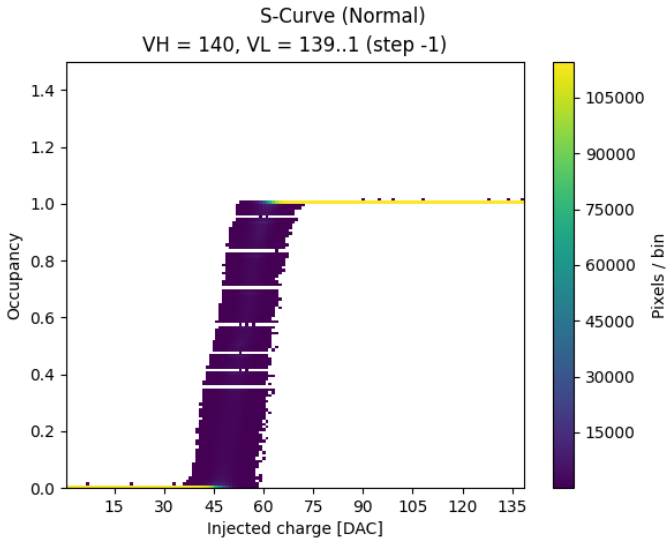

Figure 5.10: S-curves of all pixels of the Normal FE with an injection pulse of 140 DAC.

For the greater (higher) injection height, 8 different measurement have be actually done, each one on 28 consecutive columns and on all rows. Then data have been put together to obtain a single (summary) plot on the whole flavor. Same procedure has been preformed on the **Cascode FE**.

5.2.3.2 Cascode FE

Cascode FE is the second flavor and like **Normal FE** it consists of 512 rows (0-511) and 224 columns (224-447) for a number of total pixels equal to 114.688. Also for this study (measurement) the same values' registers of the setting used during the Test Beam in Desy (table 5.1) have been used and there weren't find

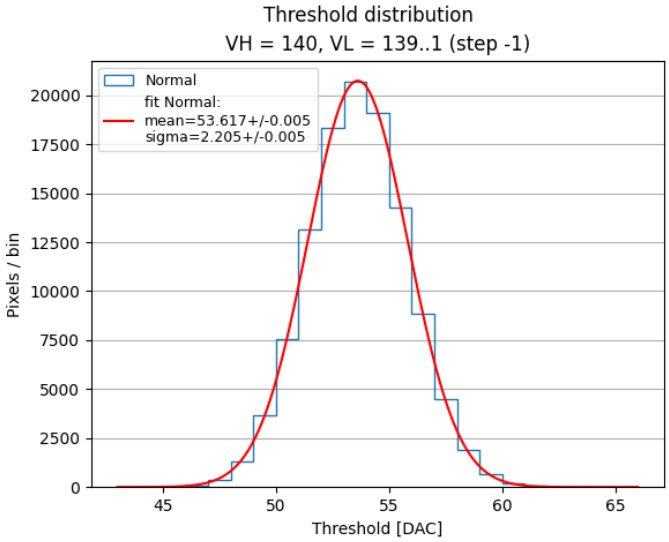

(a) VH = 140 DAC

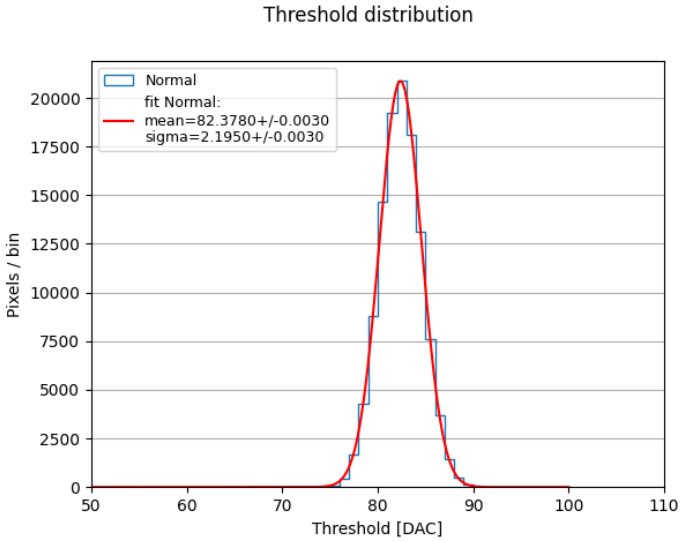

(b) VH = 200 DAC

Figure 5.11: Threshold distributions of **Normal** flavor before and at the maximum saturation, respectively.

noisy pixels. In figure **??** on page ?? the S-curves of all pixels ar showed.

The fit of the threshold distributions instead, are showed in figure 5.13 on page 32.

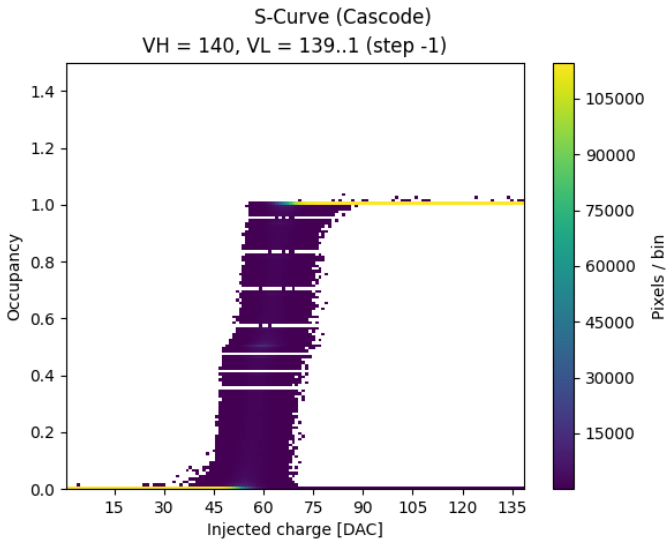

Figure 5.12: S-curves of all pixels in the **Cascode** flavor with an injection pulse of 140 DAC.

5.2.3.3 HV-Cascode FE

The third flavor is **HV-Cascode FE** where HV stands for **High Voltage** and it is formed (consists) of 512 rows (0-511) and 32 columns (448-479) for a total number of pixel equal to 16384. Also for these last two flavors, the main chip registers are set with the same values tested and used during the Test Beam (@Desy). They are reported in table 5.2.

Registri	Default Settings ("GOE")
ITHR	30
IBIAS	60
VRESET	100
ICASN	8
VCASP	40
VCASC	228
IDB	100
ITUNE	53
VCLIP	255
ICOMP	80
IDEL	88
IRAM	50

Table 5.2: Settings of the main registers used for the W14R12 chip, for the HV's flavors, during the Test Beam in Desy.

As we can see from the plot of the alle S-curves in figure 5.14 on page 33, with these choices of values' registers, there were a lot of noisy pixels, but at this stage of measurements, they were not masked.

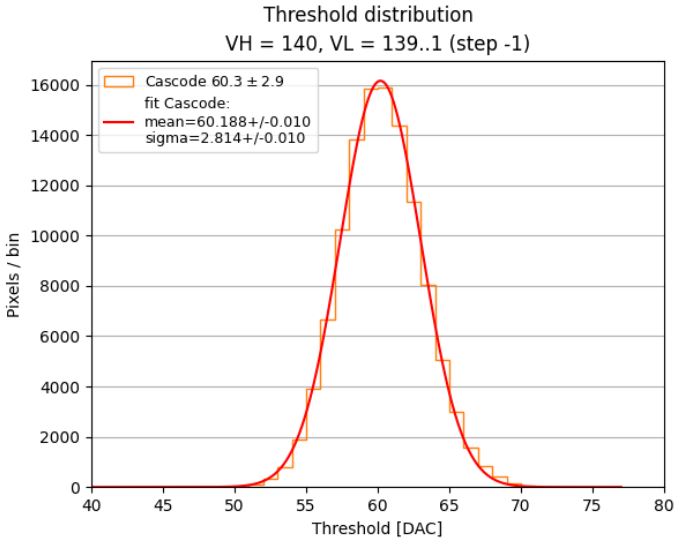

(a) VH = 140 DAC

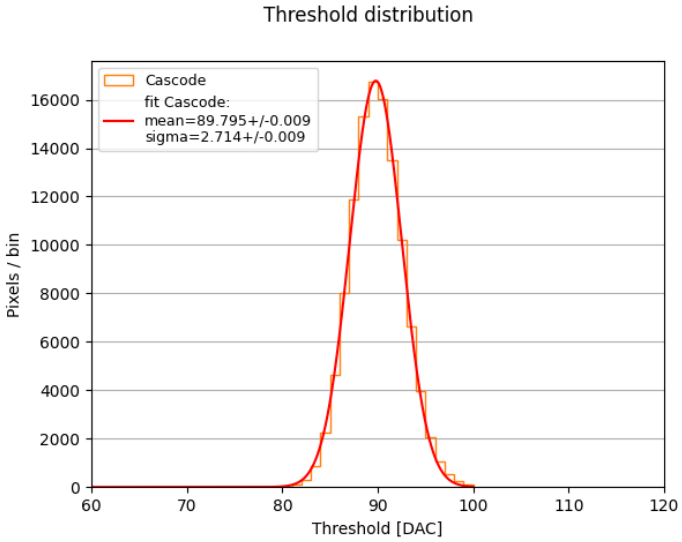

(b) VH = 200 DAC

Figure 5.13: Threshold distributions of **Cascode** flavor before and at the maximum saturation, respectively.

In figure 5.17 on page 36 are showed the fit of the threshold distributions for the two different injections pulse.

5.2.3.4 HV-Normal FE

The fourth and last flavor is the **HV-Normal FE** which consists of 512 rows (0-511) and 32 columns (479-511) for a total number of pixel equal to 16.384. The

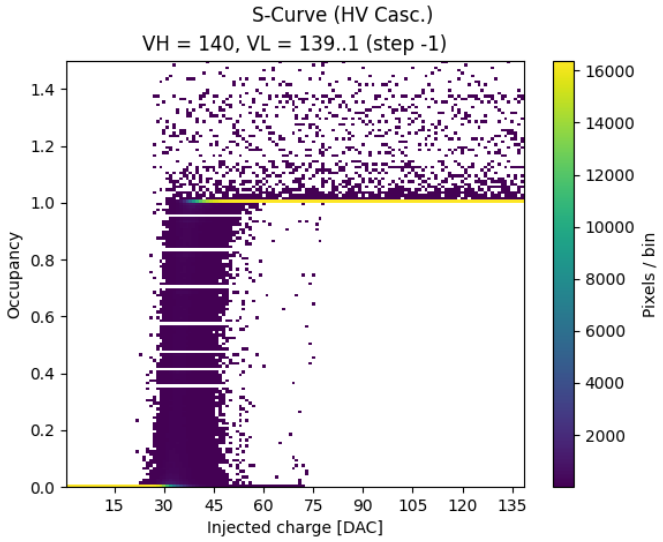

Figure 5.14: S-curves of all pixels in **HV Cascode** flavor with an injection pulse of 140 DAC.

main registers have been set with the values reported in table 5.2 on page 31. In figure 5.16 on page 35, the S-curves of all pixel in the flavor. Also here we can see that there were some noisy pixels unmasked. Moreover, in this final flavor, the last 16 columns were not working and as a matter of fact they had return a peak of threshold near the value 0, which is excluded from the threshold distributions plots.

So actually in this part of the matrix, the real number of pixel studied was the half of the total, such as 8192 pixels.

In figure 5.17 on page 36 the fit of the threshold distributions for the two different values of injection height are reported.

5.2.4 Noise and Equivalent Noise Charge (ENC)

5.2.5 Curve del Time Over Threshold (TOT) e fit

5.3 Caratterizzazione con le sorgenti radioattive

Fe55, Am241, Cd109, Sr190

5.3.1 Calibrazione della capacità di iniezione

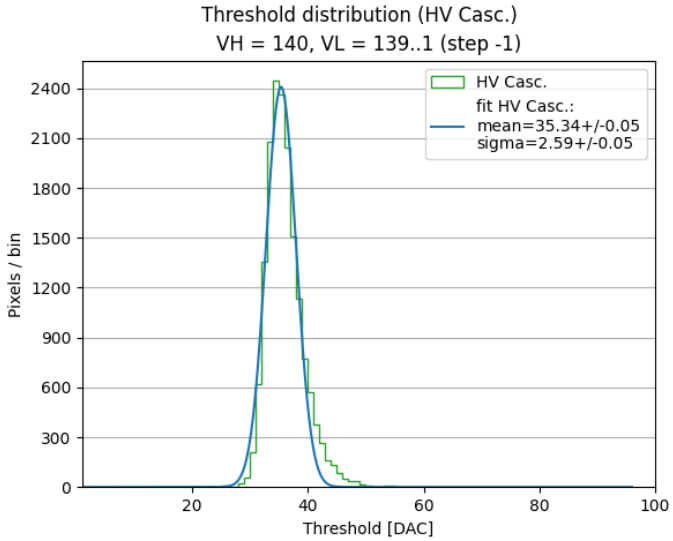

(a) VH = 140 DAC

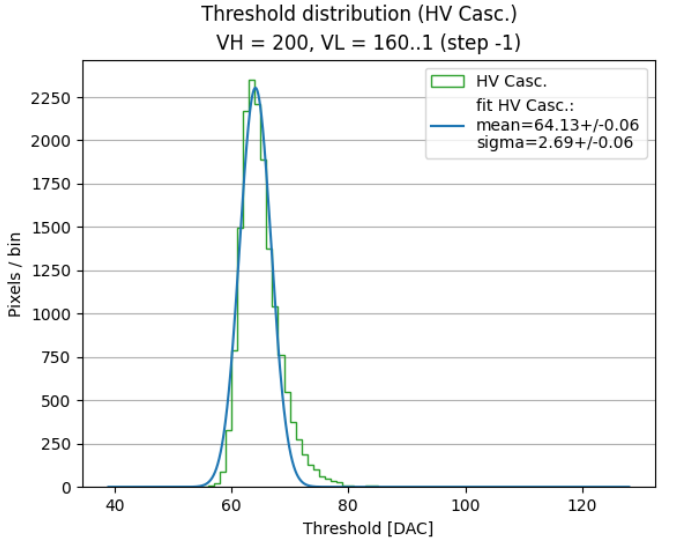

(b) VH = 200 DAC

Figure 5.15: Threshold distributions of **HV Cascode** flavor before and at the maximum saturation, respectively.

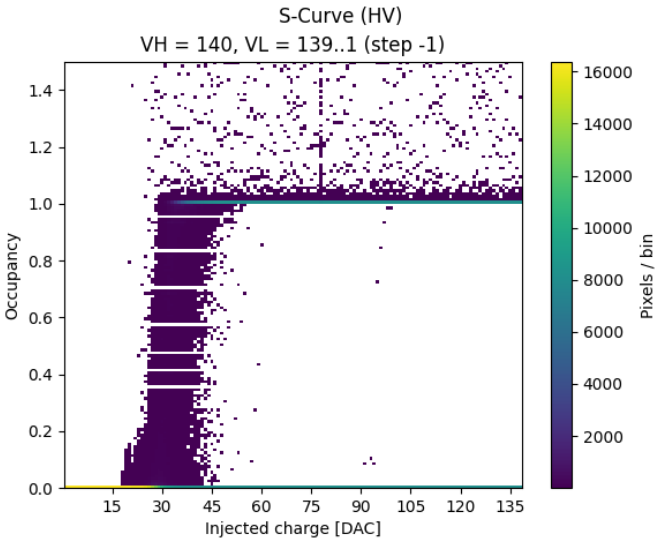

Figure 5.16: S-curves of all pixels in **HV Cascode FE** with an injection pulse of 140 DAC.

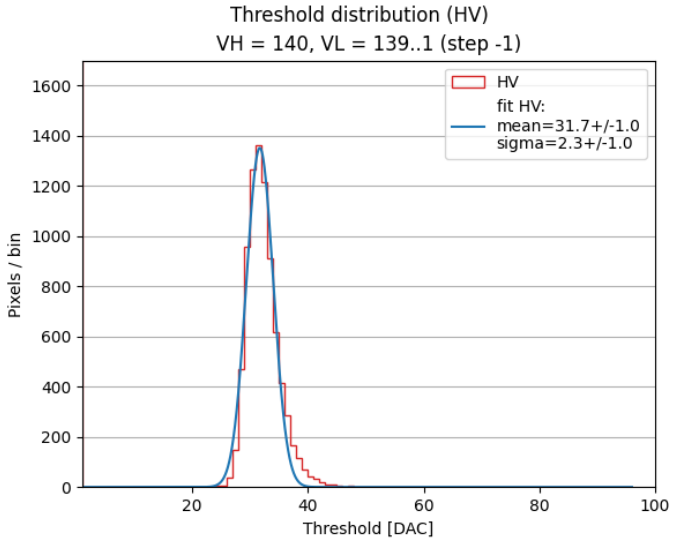

(a) VH = 140 DAC

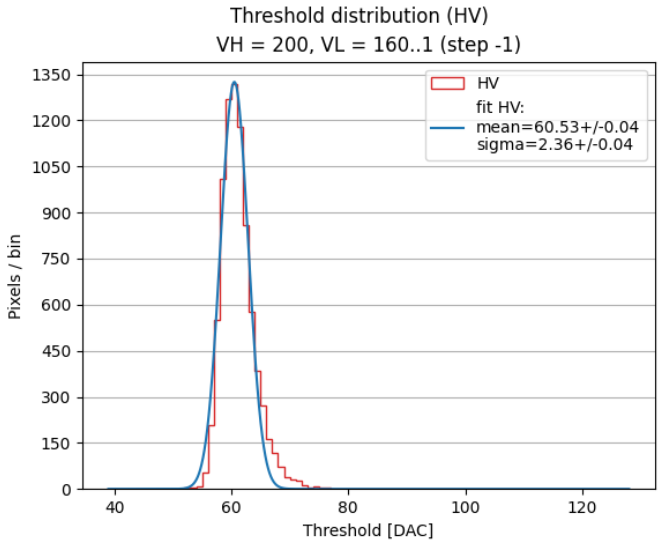

(b) VH = 200 DAC

Figure 5.17: Threshold distributions of **HV** flavor before and at the maximum saturation, respectively.

6. Conclusions